

THE SOURCE STRUCTURE OF 0642+449 DETECTED FROM THE CONT14 OBSERVATIONS

MING H. XU^{1,2}, ROBERT HEINKELMANN², JAMES M. ANDERSON², JULIAN MORA-DIAZ², HARALD SCHUH^{2,3}, AND GUANG L. WANG¹

¹Shanghai Astronomical Observatory, Chinese Academy of Sciences, No. 80 Nandan Raod, 200030, Shanghai, China; mhxu@shao.ac.cn

²DeutschesGeoForschungsZentrum (GFZ), Potsdam, Telegrafenberg, 14473 Potsdam, Germany

³Institute of Geodesy and Geoinformation Science, Technische Universität Berlin, Straße des 17. Juni 135, 10623, Berlin, Germany

ABSTRACT

The CONT14 campaign with state-of-the-art VLBI data has observed the source 0642+449 with about one thousand observables each day during a continuous observing period of fifteen days, providing tens of thousands of closure delays—the sum of the delays around a closed loop of baselines. The closure delay is independent of the instrumental and propagation delays and provides valuable additional information about the source structure. We demonstrate the use of this new “observable” for the determination of the structure in the radio source 0642+449. This source, as one of the defining sources in the second realization of the International Celestial Reference Frame (ICRF2), is found to have two point-like components with a relative position offset of -426 microarcseconds (μas) in right ascension and -66 μas in declination. The two components are almost equally bright with a flux-density ratio of 0.92. The standard deviation of closure delays for source 0642+449 was reduced from 139 ps to 90 ps by using this two-component model. Closure delays larger than one nanosecond are found to be related to the source structure, demonstrating that structure effects for a source with this simple structure could be up to tens of nanoseconds. The method described in this paper does not rely on a priori source structure information, such as knowledge of source structure determined from direct (Fourier) imaging of the same observations or observations at other epochs. We anticipate our study to be a starting point for more effective determination of the structure effect in VLBI observations.

Keywords: astrometry — galaxies: nuclei — quasars: individual (0642+449)

1. INTRODUCTION

Radio galaxies and quasars have radio-emitting structure that can be conveniently divided into two categories: extended structure, the dimensions of which range from 10^3 pc to even 10^6 pc, and compact structure, with dimensions typically ranging from 1 pc to 100 pc (Kellermann & Owen 1988). Extragalactic radio sources with compact structure are used to realize the fundamental Celestial Reference Frame with axis stability at the level of ten microarcseconds (μas) by very long baseline interferometry (VLBI) observations (Ma et al. 1998; Fey et al. 2015). Given that the typical distance to these sources is at the level of 10^9 pc, the compact structure should have angular dimensions of 0.2–20 milliarcseconds (mas), as shown in images of astrometric sources from astrophysical imaging studies (e.g., Charlot 1990a; Ojha et al. 2004, 2005; Piner 2007; Lister et al. 2009; Charlot 2010; Lister et al. 2013). For example, survey images of 91 compact sources obtained from VLBI observations at 5 GHz by Taylor et al. (1994) showed that only eight sources had a structure smaller than one

milliarcsecond. The effects of source structure on source position determined from VLBI observations were studied and demonstrated in a series of studies (e.g., Whitney et al. 1971; Fey & Charlot 1997, 2000; Feissel-Vernier 2003; MacMillan 2007; Malkin 2008; Moór et al. 2011). Recently, by observing four close radio sources in the second realization of the International Celestial Reference Frame (ICRF2) for five times over one year, Fomalont et al. (2011) found that the radio flux intensity maximum could follow a jet component rather than stay close to the radio core. Their study suggests that if the jet component gets fainter than the radio core or if they get completely separated at some time, significant position variations will occur at the level of 0.1 mas yr^{-1} or even larger.

The study of the source structure effect on VLBI observables was pioneered by Thomas (1980). A significant effort was made by Charlot (1990b), who modeled the source structure corrections for VLBI group delay and phase rate observables based on the brightness distributions of the sources. Many studies then attempted to

introduce the theoretical model of the structure effect into astrometric VLBI data analysis based on images of sources (e.g., Campbell, Schuh & Zeppenfeld 1988; Charlot, Lestrade & Boucher 1988; Tang & Rönnäng 1988; Ulvestad 1988; Zeppenfeld 1991; Charlot 1993; Gontier et al. 1993; Fey et al. 1996; Petrov 2007). For example, Sovers et al. (2002) applied it to a series of ten of the Research and Development VLBI (RDV) sessions, and the results showed that the weighted delay residuals could be reduced. An example of the application of the theoretical model to the European geodetic VLBI sessions was tested by Tornatore & Charlot (2007).

There are, however, several points that presently limit the application of this model for the correction of the structure effect. First, the source structure effect is very sensitive to a slight change in the brightness distribution. Unfortunately, the time histories of available images for most sources are quite sparse, and in the foreseeable future it is almost impossible to make images on regular basis at intervals of much less than a year for so many sources in the astrometric catalog unless astrometric/geodetic observations themselves will be scheduled in a suitable way and sufficient efforts of making images will be made. Secondly, even when images made several months apart from each other are available, the stationary reference point in these images can be hard to recognize if the radio flux intensity maximum observed by VLBI is dominated by a jet component. Consequently, in standard astrometric/geodetic VLBI data analysis, the source structure effect has not actually been handled so far. The source structure effect is still very important and challenging for the astrometric VLBI, as shown in simulation studies (Shabala et al. 2015; Plank et al. 2016). If VLBI is to achieve its full potential of the realization of the extragalactic Celestial Reference Frame with accuracy of the microarcsecond level and that of the Terrestrial Reference Frame with accuracy of the millimeter level, it is necessary to study and handle the source structure effect more effectively based on the astrometric observations themselves. These are the purposes of this paper.

In this paper we perform an initial analysis to determine how well source structure can be determined directly from the geodetic VLBI observables themselves¹. We aim to develop an alternative method for studying the structure effect that should be simple, easy to

implement, and applicable for general historical and future geodetic VLBI observations, including many of the oldest observations (back to the 1970s) for which the visibility datasets are no longer available. Although a self-calibration and Fourier imaging analysis of the visibility data can give superior results for determining source structure, that approach is time and computing resource intensive, it requires large amounts of software not currently implemented in geodetic analysis packages, it requires that the observations were conducted in a manner suitable for imaging, which is frequently not the case for historical geodetic VLBI sessions, and it will be difficult, yield sub-optimal results, or even be impossible for the historical experiments that no longer have archived visibility datasets.

Therefore we defer our structure analysis based on imaging for a future publication, and we make use of the closure delay, the sum of the delays around a closed loop of baselines, as a new observable and propose a method to use this new observable for the determination of the source structure effect on the astrometric VLBI observable. We calculate the closure delays, investigate the characteristics of the source structure, and then solve for the source structure effect on each observable. The source structure can be finally obtained and the source structure effect can be determined. The source 0642+449, one of the ICRF2 defining sources, is selected as a demonstration case for this method.

The systematical analysis of closure delay requires a consistent definition and a careful discussion of closure delay, which are presented along with its calculating model in Section 2. The data used here, the CONT14 observations, and the overall statistics of the closure delay of source 0642+449 are introduced in Section 3. Section 4 discusses the method that was used to solve for the source structure effect on each observable based on the knowledge from Section 3. The results, describing the structure of this source, are shown in Section 5, and the final model is presented in Section 6. Conclusions and discussion are given in the last Section.

2. MODEL OF CLOSURE DELAY

The closure phase, unaffected by instrumental and atmospheric instabilities, was recognized as a good observable for the study of source structure first by Jennison (1958) and later by Rogers et al. (1974). A method for recovering the brightness distributions of compact radio sources from VLBI observations of closure phase, together with the measured visibility amplitudes, was developed to make images at the scale of milliarcseconds (Readhead & Wilkinson 1978) and used to obtain valuable maps for 45 objects by Pearson & Readhead (1981, 1988) in the early stage of VLBI imaging. The methods using the closure phase for recovering the bright-

¹ Geodetic/astrometric VLBI observables are the baseline-based group delays and phase rates determined per scan within a geodetic VLBI experiment. The International VLBI Service for Geodesy and Astrometry (IVS) coordinates archives of geodetic VLBI experiment observables (see <http://ivscc.gsfc.nasa.gov/products-data/data.html>), but visibility datasets are normally not made available for analysis.

ness distribution of a radio source were called *hybrid-mapping based on closure quantities*, which was widely applied for the study of source structure (see [Pearson & Readhead 1984](#), and references therein). In terms of independence from instrumental and atmospheric instabilities and sensitivity to source structure, closure delay has similar characteristics to closure phase. The closure delay was used for evaluating the performance of the structure models in the past ([Charlot 1990b](#)), but our method will use it in a more direct way. For the first time, the definition and the model of closure delay is given here.

For a triangle of 3 stations, a , b , and c , the closure delay is defined for an individual wavefront by

$$\tau_{abc} \equiv \tau_{ab} + \tau_{bc} + \tau_{ca}, \quad (1)$$

where, for instance, τ_{ab} is the delay observable from station a to station b , and τ_{bc} is the delay observable from station b to station c , for the same wavefront received by three stations. Equation (1) depicts the scenario in which the same wavefront passes stations a , b , and c in some arbitrary sequence. The closure delay, for an ideal point source, is independent of any station-based or source-based effect and should be zero if there is no observational noise. For sources with detectable structure, as expected even for most astrometric sources, the group delay observable depends on the observing frequency and the baseline length and orientation differently from the group delay behavior for a point source. In general, the change in the group delay will be different for each baseline in the closure delay triangle dependent upon the source structure, and the resulting closure delay will be non-zero. Therefore, variations in the closure delays sufficiently far away from zero that they are unlikely to be caused by random measurement noise should, in principle, only be observed for sources with significant structure.

In geodetic VLBI measurements, by convention, the time tag of group delay, phase, and phase rate observables is referred to the epoch when the wavefront passes the first station in the baseline. They are implemented in the VLBI processor such that all observables in one scan have exactly the same time tag value. This means that the observables in one scan are usually not related to the same wavefront and allowance must be made for the delay of the arrival of the same wavefront at the different stations. Moreover, the baseline name is made up of two stations' names in the alphabetical order, so that τ_{ca} should be replaced with the actual geodetic VLBI observables on that baseline, $-\tau_{ac}$. Therefore, to the accuracy of the second order in delay, the closure delay at reference epoch t is calculated from

$$\tau_{abc}(t) = \tau_{ab}(t) + [\tau_{bc}(t) + \dot{\tau}_{bc}(t) \cdot \tau'_{ab}(t) + \frac{1}{2} \ddot{\tau}_{bc}(t) \cdot \tau'_{ab}(t)^2] - \tau_{ac}(t), \quad (2)$$

where a prime on a delay symbol indicates an absence of dependence on station clock offset, that is, referring to the geometric delay, and a superposed dot and double superposed dots denote differentiation with respect to time once and twice, respectively.

For a goal of 1 ps accuracy of the closure delay, the third term inside the bracket of Equation (2) is smaller than 0.1 ps and is therefore negligible, since for ground-based VLBI the magnitude of the group delay is at the level of 0.02 s and that of the second order derivative is at the level of 10 ps s⁻². Since the magnitude of the first order derivative is at the level of 1 μ s s⁻¹, the second term inside the bracket has the magnitude of about ten nanoseconds (ns) and should be calculated as accurately as possible. The $\dot{\tau}_{bc}(t)$ term can be calculated from the theoretical model, which may have to ignore the rate of change of the propagation delay; it can be derived more accurately from the phase rate observable and the ionospheric delay rate, both of which are available for International VLBI Service for Geodesy and Astrometry (IVS, [Schuh & Behrend 2012](#)) VLBI observations. All clock offsets or jumps larger than 0.1 μ s should be taken into account for the geometric delay, $\tau'_{ab}(t)$, in Equation (2) if it is calculated from the group delay observable.

Following the conventions in geodetic VLBI measurements of the time tag and of the baseline's name, the closure delay in this paper will be referred to the same epoch as that of the three observables in the triangle and be labeled by the names of the three stations in alphabetical order. In this case, the baseline between the first station and the third station in a triangle will always contribute to the closure delay calculated from Equation (2), in contrast to other two baselines, with a negative sign.

3. CLOSURE DELAY OF SOURCE 0642+449

The data from CONT14² observations ([Nothnagel 2015](#)) at X band were used. CONT14 is a campaign of continuous VLBI observations, conducted by the IVS from 00:00:00 UT on 2014 May 6 to 00:00:00 UT on 2014 May 21. It is a continuation of the series of continuous VLBI observations over 15 days that were observed every three years since 2002. With a network of ten stations in the northern hemisphere and seven in the southern hemisphere at sixteen sites³, this campaign

² <http://ivsc.gsfc.nasa.gov/program/cont14/>

³ Two stations, HOBART12 and HOBART26, are located at the Hobart site in Australia.

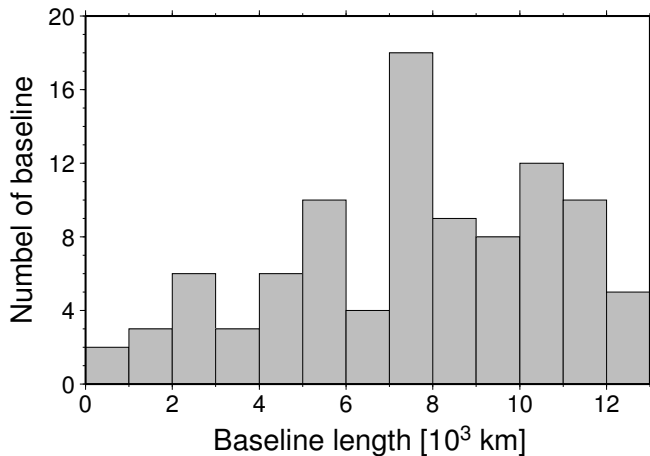


Figure 1. The baseline lengths of the observing network of source 0642+449 in CONT14. There were in total 15 stations observing this source, and 96 baselines were correlated.

was intended to acquire state-of-the-art VLBI data over a time period of 15 days with the highest accuracy that the then existing VLBI system was capable. In these continuous observations there are several sources with about one thousand observables per day, which makes the CONT14 observations considerably valuable for the study of source structure.

The radio source 0642+449 was selected as the target of our study. It was observed in 512 scans by 15 stations in the CONT14 campaign (only the two southernmost stations at the Hobart site could not observe this source), and has in total 11 027 pairs of usable (quality codes⁴ smaller than 8) group delay and delay rate observables at X band. In total, 22 154 closure delays were calculated from this data set and provided important statistics of the performance of this individual source. As the number of triangles is about two times that of group delay observables, each individual group delay on average is involved in six triangles. The resulting triangles have 350 different kinds of geometry. There are in total 96 baselines with lengths ranging from 900 km to 12 600 km as shown in Figure 1. This widely-spanned baseline length provides a good uv coverage, eventually facilitating the detection of the source structure at a variety of scales.

Multiband group delay ambiguities of 100 ns or 50 ns, determined by inspecting the closure delay, were fixed for three group delays for the baseline WESTFORD–YARRA12M on the 6th, 10th, and 11th of May. After this change to the CONT14 observations, the 22 154 closure delays were then recalculated. Six closure delays with absolute value larger than 28 ns were subse-

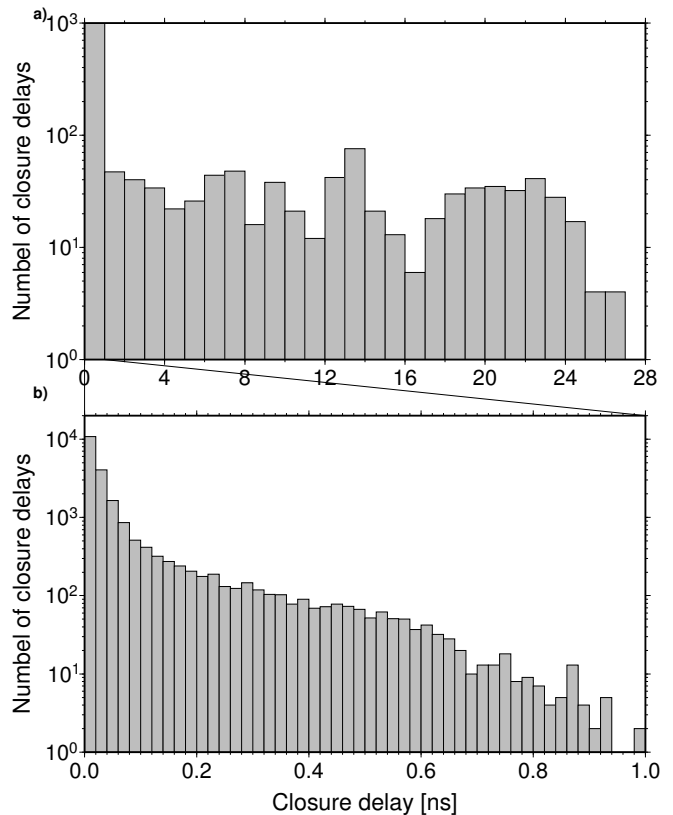


Figure 2. The absolute magnitude distribution of closure delay of the source 0642+449. The subplot *a* shows the distribution of closure delay in the whole range from 0 ns to 28 ns with the bin width of 1 ns, and the subplot *b* shows, with a smaller bin width of 20 ps to demonstrate more detail, the distribution in the main range from 0 ns to 1 ns which has been out of the axis limit as one bin in the subplot *b*.

quently excluded as outliers in the analysis here. No other changes to the data were made and no additional points were excluded from analysis. Figure 2 shows the distribution of the absolute magnitudes of the 22 148 closure delays. Approximately 49% of the triangles have closure delays of absolute value smaller than 20 ps, and 67% of triangles have closure delays of that smaller than 40 ps. As Figure 2 shows, there is a rather flat distribution in each of the subplots: the one in subplot *a* lies in the range larger than 1 ns containing 759 closure delays; and the one in subplot *b* lies in the range of 0.1 ns to 0.9 ns, which has 16% of triangles. The mean value and the standard deviation of closure delays for the whole set of triangles is -0.02 ns and 2.668 ns, respectively, and 0.3 ps and 139 ps, respectively, for the set in the range 0 to 1.0 ns. The statistics and the distribution of closure delay demonstrate that source 0642+449 to some extent performs well for a geodetic source showing closure delays of less than 20 ps for half of the triangles, but it is not as compact as a point-like source. Furthermore, there are about 759 closure de-

⁴ <http://lupus.gsfc.nasa.gov/global/ngs-doc.html>

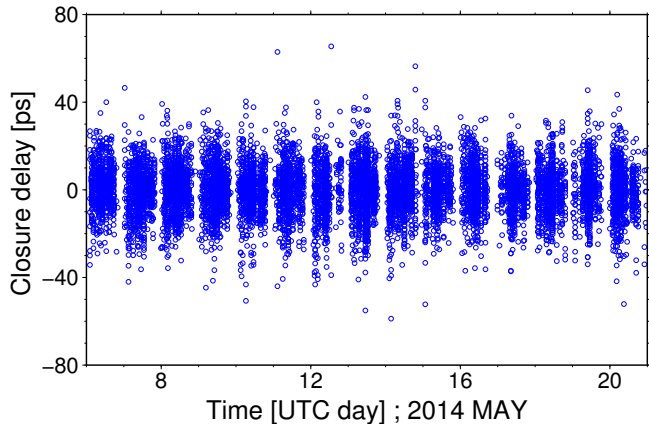


Figure 3. The closure delays of 0727-115 over 15 days. There is absolutely no triangle with closure delay of magnitude larger than 70 ps, and most triangles are with closure delays of magnitude smaller than 30 ps.

lay magnitudes above 1 ns, suggesting that about 127 group delays (based on the average number of triangles each single group delay is part of), about 1 % of the total observables for this source, sense exceptionally large structure effects. For a comparison to demonstrate the measurement noise in VLBI observables, the standard deviations of closure delays for unresolved sources, such as 0016+731 and 0727-115, were calculated as well. Source 0016+731 has about 23 300 closure delays and 0727-115 has about 11 200 closure delays. The standard deviation for source 0016+731, which showed a little resolved structure, is about 11 ps, and that for source 0727-115 is about 8.0 ps. Figure 3 shows the closure delay distribution over 15 days. Geodetic VLBI observations are scheduled with different observing durations for each station and each expected source brightness to achieve a uniform signal to noise ratio for all observations, so we assume that the $8.0/1.7=4.6$ ps standard deviation for 0727 – 115 represents the upper limit to the typical measurement noise for all sources in CONT14 observations, and the vast majority of the 139 ps scatter in the 0642 + 449 closure delays cannot be explained by the measurement noise.

3.1. Triangles with three short baselines

The closure delays of triangles with all three baseline lengths⁵ smaller than 7100 km were investigated. In Figure 4, the closure delays of these triangles are shown as red circles connected by dashed lines. The time in hours on the X axis is the GMST time of the observation for each triangle epoch to show observations over the fifteen days in an overlapping 24-hour plot. The same tech-

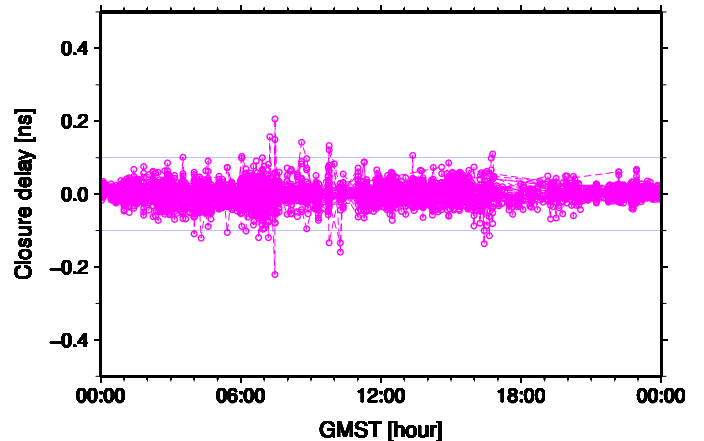


Figure 4. The closure delays of triangles with all three baselines shorter than 7100 km, which in total have 42 different geometries. All points are connected by dashed lines to show whether there are points out of the chosen axis limit. This is applied to all figures that show the closure delay or the source structure effect in the paper. For this case, not a single closure delay is out of the axis limit.

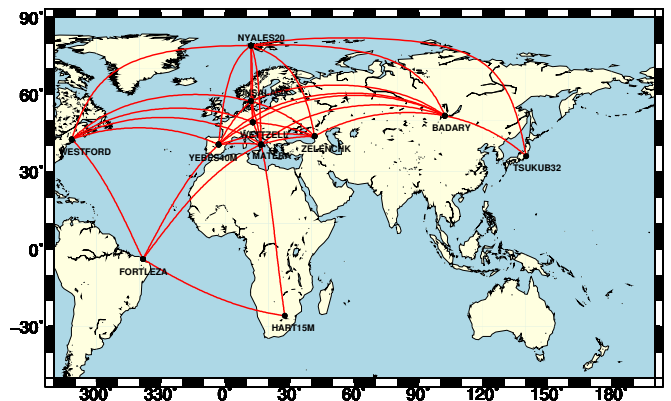


Figure 5. The triangles with all three baselines shorter than 7100 km.

nique is applied in the following figures of closure delays. There are in total 6611 closure delays for these small triangles, and the standard deviation is about 21.7 ps. Figure 5 geographically shows these small triangles⁶. The magnitudes of the closure delays of these triangles are mostly smaller than 40 ps. There are 24 closure delays with magnitudes larger than 0.1 ns, and if we constrain the small triangles to having baseline lengths shorter than 7000 km, the magnitudes of the closure delay are all smaller than 0.1 ns.

3.2. Triangles with one long and common baseline

⁵ Total baseline length is used throughout the paper as a proxy for projected baseline length.

⁶ We should notice that there are more short baselines than shown in Figure 5, since there are some isolated short baselines unable to form such a small triangle.

The closure delays of triangles that contain one long baseline and two short baselines were investigated. In the CONT14 network, six stations are densely located in the European region so that one can make use of them to construct a good set of triangles for this investigation. Figure 5 suggests that the long baseline should be BADARY–WESTFORD, since the European region locates almost in the middle of it. The length of baseline BADARY–WESTFORD is approximately 8700 km. ZELENCHK connects to BADARY with the baseline length of approximately 4400 km, but to WESTFORD about 7800 km, a little longer than 7100 km; the other five European stations connect to both with baselines shorter than 7100 km. Figure 6 shows the closure delays with respect to the GMST time of the resulting six kinds of geometry using six colors. Figure 7 shows the geographic positions of these eight stations and the triangles with these six different geometries. Aside from the points outside the Y axis limits, these six sets of closure delays roughly have the same pattern, two peaks happening around 03:00 and 15:00 with magnitude of approximately 0.5–0.7 ns. When WESTFORD is the third station in the triangle, the sign of the peaks is opposite to that when WESTFORD is the second⁷. Considering that baseline BADARY–WESTFORD is the only common one in these triangles and that triangles with baselines shorter than 7100 km show no closure delays larger in magnitude than 0.2 ns, it is reasonable and obvious to conclude that the systematic variation in the closure delays of these six kinds of geometry is predominately related to the baseline BADARY–WESTFORD. In addition, the closure delays of the nanosecond order and larger, which are out of the axis limit in the plot, only happened around the same GMST time of the peaks.

3.3. Triangles with the shortest baseline

As we know, the atmospheric and clock errors limit our ability to examine the structure effect on a single baseline on its own. The investigation in Section 3.2 above demonstrates the effect of source structure introduced by one long baseline by using two short baselines in the closure triangle to cancel out the atmospheric errors, clock errors, and so on, in the long baseline. The closure delays of all triangles including the smallest baseline in the CONT14 network, ONSALA60–WETTZELL, were investigated. They are shown in Figure 8 by two subplots with different scales. As there were 13 stations available to form a triangle with baseline ONSALA60–WETTZELL, we have 13 different kinds of

⁷ By the naming convention, in this case, WESTFORD can never be the first station in a baseline, and BADARY is always the first station.

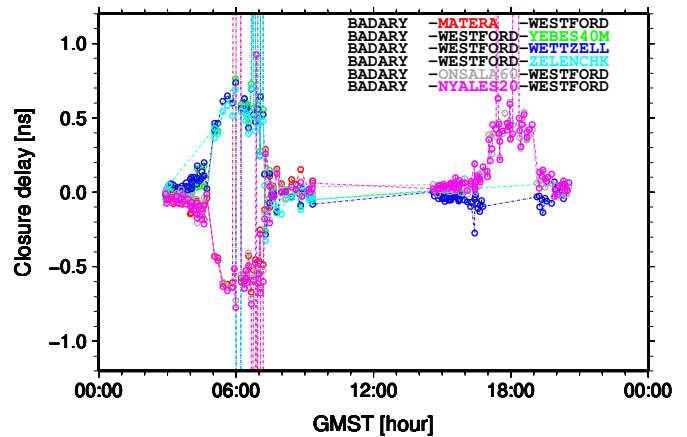


Figure 6. The closure delays of triangles with BADARY and WESTFORD and one of the six European stations. Each color corresponds to the closure delays of triangles of one kind of geometry, with the name shown on the upper right corner in the same color for the European station in that triangle. Points for the triangles with the same geometry are connected with dashed lines.

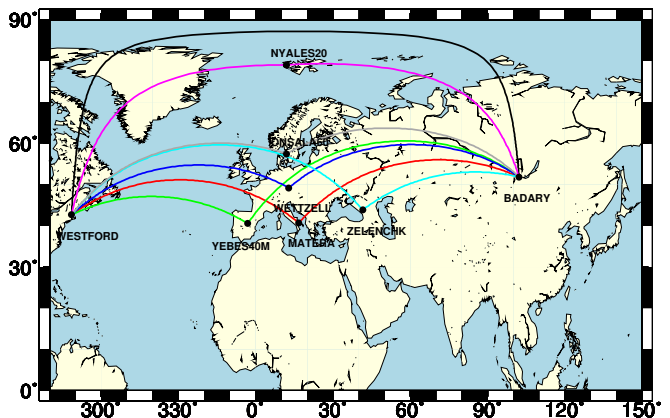


Figure 7. The geographic locations of BADARY, WESTFORD, and six central European stations. The black line is BADARY–WESTFORD; the six pairs of baselines connecting the stations BADARY and WESTFORD are shown with the same colors with that of the closure delays that they contribute to in Figure 6.

geometry for this case. The closure delays were classified and sorted by the geometry of each triangle. In this figure, the names of 13 different geometries are presented in the numerical order of the longest baseline length in the geometry, and the colors for the names of the 13 stations correspond to those of the closure delay in each of the subplots. Most closure delays of these triangles are very small, at the level of tens of picoseconds, if the longest baseline in the triangle is shorter than 7600 km. The magnitudes of the closure delays become larger as the baseline lengths in the triangles continue to increase, and eventually systematic variations appear. In this case, the variations are much more complicated than

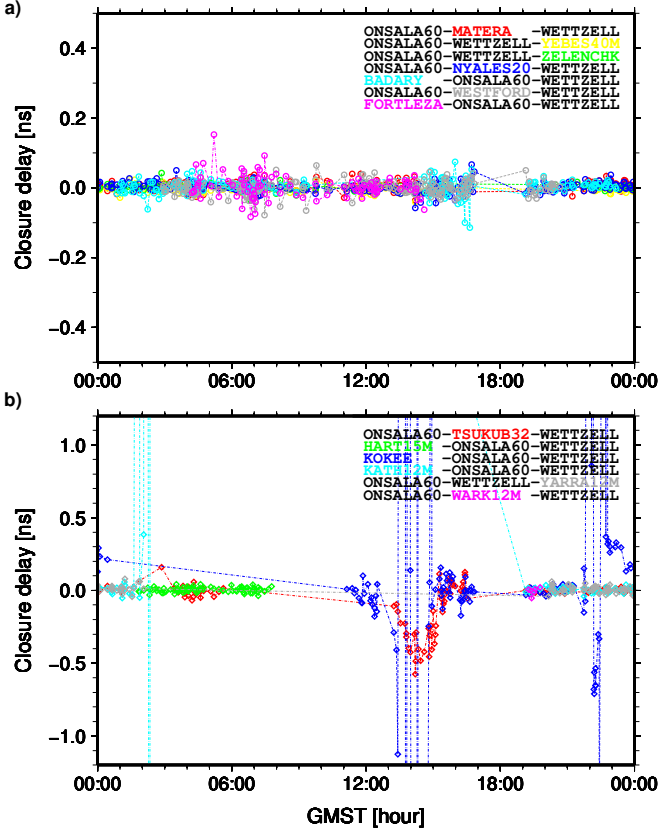


Figure 8. The closure delays of all triangles that contain the baseline ONSALA60–WETTZEILL. Since 15 stations observed this source, there are 13 station available to join these two stations to construct a triangle. Subplot a shows the closure delays with seven different third station in different colors, while subplot b shows with a larger axis limit, closure delays from triangles using the remaining six stations. The names of 13 different kinds of geometry in both subplots are presented in the numerical order of their longest baseline lengths. For each geometry, the name of the third station is presented in the color of its closure delay.

that for triangles with only one long baseline as shown in Figure 6. Closure delays larger than 1 ns appear only when there are long baselines in the triangle and where apparent systematic variations for short baseline triangles occurred.

4. METHOD TO SOLVE TRIANGLES

As discussed in Section 2, the measured closure delay is due to the observational noise and the source structure effect that is baseline dependent. Then

$$\tau_{abc} = \delta\tau_{ab} + \delta\tau_{bc} - \delta\tau_{ac} + \sum_{i=1}^3 \epsilon_i, \quad (3)$$

where $\delta\tau_{ab}$, $\delta\tau_{bc}$, and $\delta\tau_{ac}$ are the source structure effects on the three baselines, and ϵ_i is the measurement noise in the i -th baseline of that triangle. It is reasonable to assume here that measurement noises are random at the

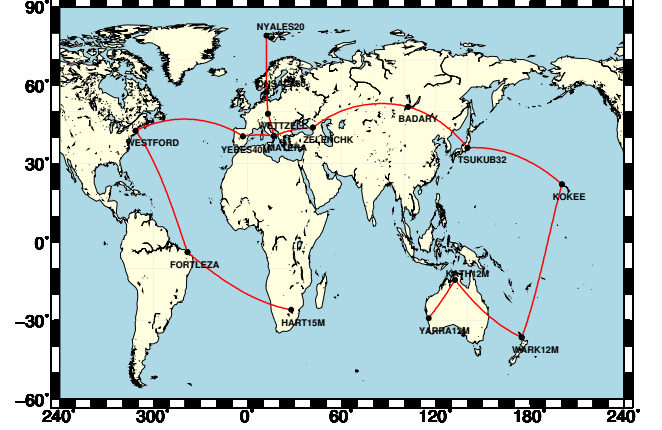


Figure 9. An example of a complete connection of the fifteen-station network by a minimal number of < 7100 km long baselines. To solve for the baseline delays using closure delay in one scan, these selected baselines are set to have zero source structure effect in that scan. This kind of connection and its role is designated as connection in the paper.

level of a few picoseconds, which has been demonstrated by the closure delays of unresolved sources.

In an array of N stations, there are at most $N(N-1)/2$ baselines and $N(N-1)(N-2)/6$ closure delay relations. But only $(N-1)(N-2)/2$ of these relations are independent (Pearson & Readhead 1984). There are therefore $(N-1)$ too few closure delays to determine the source structure effect for each standard baseline-delay observable, and an independent estimate of the structure delay on $(N-1)$ baselines has to be derived. The investigations in Section 3 give insights to this and the proposed method uses the assumption that source 0642+449 is a point-like source with respect to the baselines shorter than a certain value. We then choose 7100 km as the threshold and select a necessary and minimum number of < 7100 km baselines to connect as many stations as possible in each scan. The structure effects on these selected baselines are assumed to be zero. Taking a fifteen-station array as an example, ideally there are fourteen baselines shorter than 7100 km connecting fifteen stations as a complete connection shown in Figure 9. Setting the source structure effect on these selected baselines to be zero allows us to solve for the structure effects on other baselines utilizing the closure delays.

To find such a kind of a complete connection could be very challenging in some cases. This is the case for the southern stations. Three southern stations, KATH12M, YARRA12M, and WARK12M, can be connected to the whole network through such a connection only if at least one of the baselines KOKEE–WARK12M (6600 km) and KATH12M–TSUKUB32 (5500 km) is available. If both of these two baselines get lost in a scan, it is thus impossible to solve all the big triangles related to these three stations. This is also one of the reasons for choosing 7100

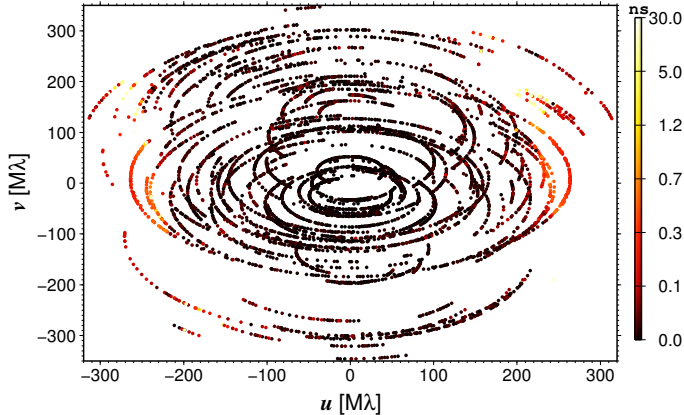


Figure 10. Coverage of the Fourier domain (uv coverage) of the CONT14 observations of 0642+449 at 8.4 GHz ($\lambda = 3.6$ cm), plotted in units of Mega lambda. Color marks the absolute magnitude of the source structure effect on each of 8492 observables derived from closure delays by the method introduced in Section 4.

km as the threshold for the baseline length of the connection, considering that the shortest baselines related to station HART15M, are HART15M–MATERA (7033 km) and FORTLEZA–HART15M (7025 km). Next step is to solve as many triangles as possible based on the connection with the threshold of 7100 km scan by scan.

5. RESULTS OF SOURCE STRUCTURE EFFECT

Finally, 16 941 triangles were solved and the source structure effects on 8492 baseline delays were determined based on Equation (3). In this solution, 2179 observables of short (< 7100 km long) baselines were assumed to have no source structure effect to build up the connection. Figure 10 shows the uv coverage with color marking the magnitude of the derived source structure effect on each point. In general, the source structure has a strong effect on long baselines at two opposite directions of approximately the u axis. The results are divided into two groups for the detailed study of learning the source structure effect.

First, apart from the observables selected to form the connection, the structure effects on the remaining 3443 observables of short baselines were estimated along with long baselines in the solution. The estimated source structure effects on these baselines with respect to uv position angle of baseline in the uv plane (measured North-through-East) are shown in Figure 11. All these observables without exception have very small source structure effects, and the standard deviation is about 22.7 ps, which is close to that of the closure delays of triangles with short baselines shown in Figure 4. It may be slightly larger than that of random measurement noises in VLBI measurements, partly because the measurement noise in 2179 zeroed observables were propagated into

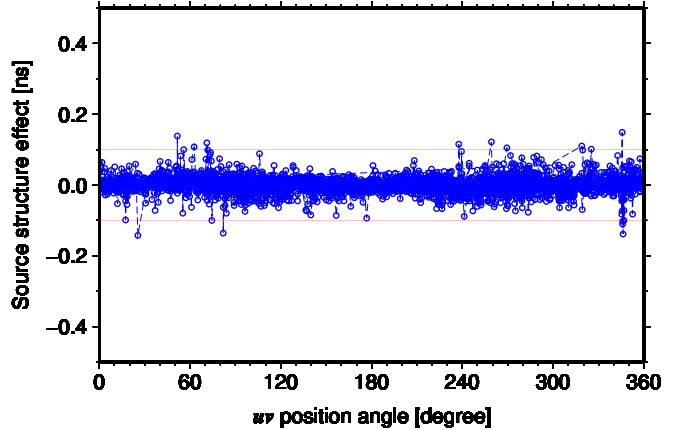


Figure 11. Derived source structure effects on 3443 observables of short baselines (< 7100 km) from the closure delays, plotted as a function of the uv position angle of baseline.

the estimated ones. There is no point larger than 0.2 ns. Therefore, the result supports the assumption of no significant structure on short baselines that has been used for the connection.

Secondly, the source structure effects for eight long baselines with significant variations are presented one by one in Figure 12 in blue dots. The patterns shown in these plots are incomplete over one circle of uv position angle, especially for the longest baselines, due to both the loss of common visibility of the source and the vulnerability of losing link to the connection. This indeed makes the identification of the source structure extremely challenging. However, it is beneficial to combine together the patterns in these plots. Two peaks for the baselines with length from 8400 km to 9600 km can be identified, appearing at the uv position angles of approximately 90° and 270° . The peak structure effect for these baselines is 0.7 ns. Moreover, there are two characteristics of the source structure that can be identified. First, apart from the points outside of the axis limit, the scatter of the structure effect is rather small along the track of the variation curve, and this should imply that the source has multiple point-like components rather than a flat brightness distribution over the extended structure. Second, the variation is symmetric over the uv position angle of one circle, and the separation between the two peaks is 180° . As a result, the source should have a symmetric brightness distribution, for example, the multiple components are in a straight line. Finally, points out of the axis limit happen exclusively on baselines longer than 9000 km where significant source structure effects occur.

6. MODELING THE SOURCE STRUCTURE OF 0642+449

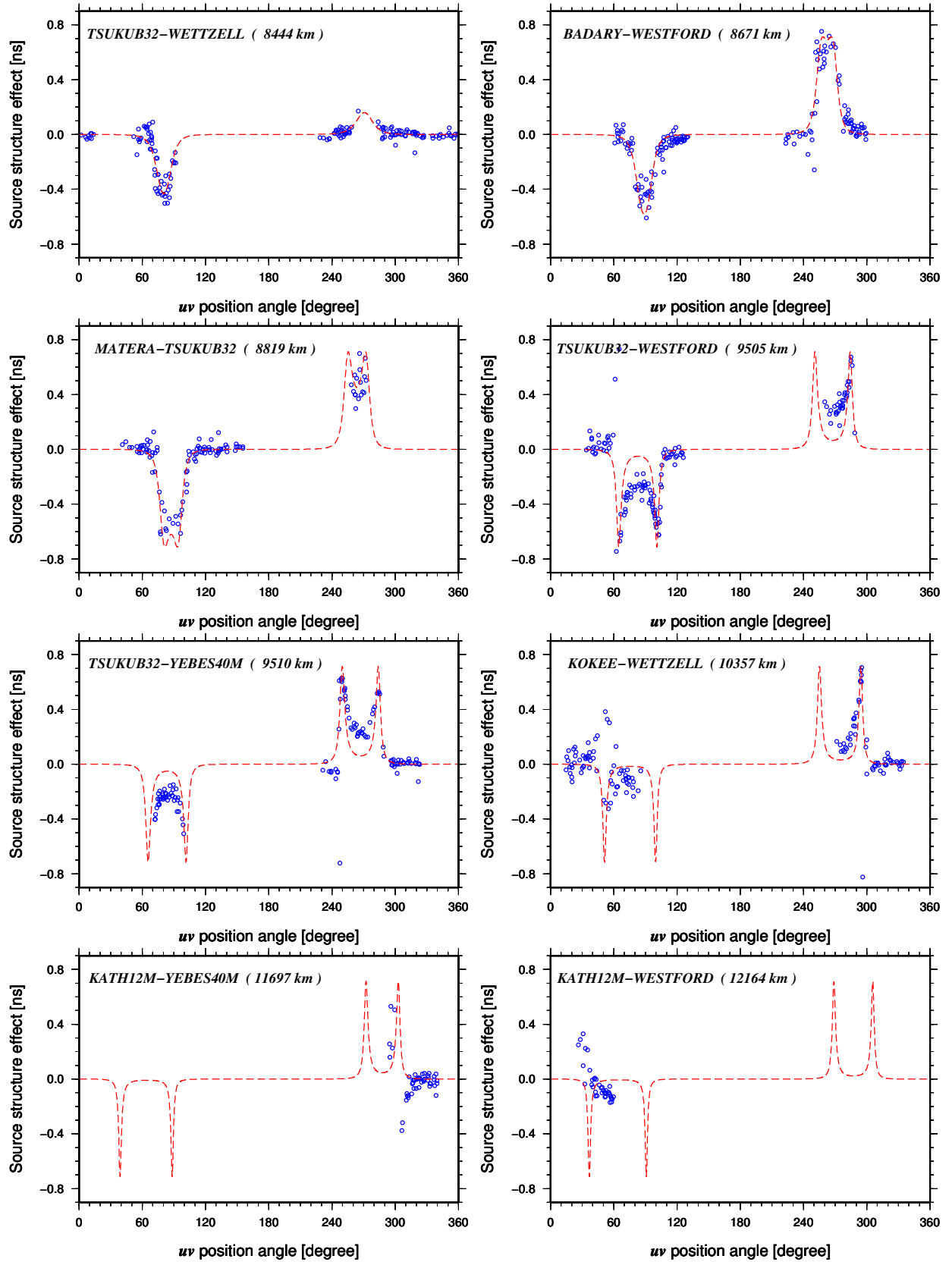


Figure 12. Derived source structure effects from the closure delay and the pattern of structure effects calculated from the two-component model as a function of the uv position angle for eight baselines with significant variations. The baseline name along with the baseline length in brackets is shown for each of the plots. The blue dots correspond to the observation points, and the complete patterns of structure effects over one circle calculated from the model are shown in red dash lines.

The examples of a double-component source and a triple-component source have been analyzed by Thomas (1980), and a double-component source has been studied in great detail by some simulations of Charlot (1990b). Based on these studies, we can determine that the source exhibits a structure with two compact components on baselines with length of around 9000 km. The ratio of the flux densities of the weaker component to the stronger one, K , is about 0.92, since the peak structure effect for these baselines is approximately 0.7 ns.

Thomas (1980) referred the source position in his model to the middle point of the separation between the two components, while Charlot (1990b) took the centroid point of brightness as the reference point. The reference point does not matter for the closure delay, but we apply the centroid model here, because we assume that observables of short baselines have zero source structure effect, and in practice they are referred very closely to the center of brightness. According to this model, the structure delay τ_s on baseline \mathbf{B} is given as

$$\tau_s = \frac{K(1-K)[1 - \cos(2\pi R)]R}{f(1+K)[K^2 + 2K\cos(2\pi R) + 1]}, \quad (4)$$

where f is the observing frequency, $R = \mathbf{B} \cdot \mathbf{S}_{12}/\lambda$, λ is the wavelength, and \mathbf{S}_{12} is the relative position vector in the uv plane of the weaker component P_2 with respect to the stronger one P_1 . This expression only accounts for the change of the projected baseline on the uv plane, i.e., the sky fringes. It assumes that the flux densities of two components do not change with frequency and observations are made on an infinitesimal bandwidth.

Since the closure delay is not sensitive to the reference point in the source structure at all, this study lets all observables refer to an unknown point, in this case to the centroid of brightness by the choice of the model, per scan. This reference point will finally be determined through VLBI data analysis. We further assume that the source structure does not change within the fifteen days of observations. A “guess” estimation for the unknown parameters in Equation (4) was made from the results of baselines with lengths from 8400 km to 9600 km derived in Section 5. The final estimation was done by model-fitting all the closure delays with magnitude smaller than 1.0 ns based on the a priori values from the guess estimation. The flux-density ratio is then estimated to be 0.916 ± 0.012 , and the relative position vector be $-426 \pm 12 \mu\text{s}$ in right ascension and $-66 \pm 19 \mu\text{s}$ in declination. According to the detected morphology, a baseline with length of 7100 km has $R = 0.41$ and the peak structure effect is only 13 ps, which explains the foundation of the assumption short baselines have no structure effect used for the connection.

One can easily compute the source structure effect for

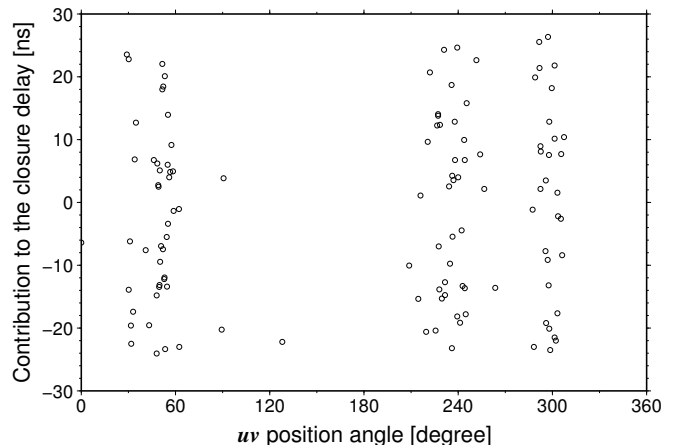


Figure 13. Distribution of the 117 observables with contribution to the closure delay larger than 1 ns.

each observable based on Equation (4) and the two-component model. The results for the eight baselines are shown in Figure 12 in red dash lines. By comparison, we found that the model fits all the baselines with length smaller than 10 000 km, but it does not fit so well for some of the longest baselines, for example baseline KATH12M–WESTFORD shown in Figure 12, where the model and the estimated structure effect just have different variations. After using the model to correct the structure effect, the standard deviation of the closure delay was decreased from 139 ps to 90 ps for all triangles with closure delay less than 1 ns, which is a significant improvement.

Another solution was done to trace the observables that cause 749 triangles to have closure delays larger than 1 ns. It is much easier to locate these observables actually, since the magnitude is so large that all triangles related to them apparently have quite large closure delays. The threshold of baseline length was then reset to a little larger than the previous one, 8000 km for the connection. The baseline with a length within this threshold should have a peak structure effect of 0.12 ns, which will corrupt the determination of the source structure effect for many observables, but facilitate locating the points with large contribution to the closure delay. This solution allows 21 700 triangles to be solved, and 117 observables have been identified with large contributions to the closure delay. Figure 13 shows the estimated closure delays of these 117 observables as a function of the uv position angle. Table 1 shows the baselines lengths of these observables. All these points systematically lie in three ranges of uv position angle, 30° – 60° , 220° – 250° , and 280° – 310° , and refer to baselines with lengths larger than 7600 km, most of them larger than 9000 km. It leads us to conclude that these large closure delays are more likely caused by the source

Table 1. Statistics of the 117 observables with contribution to the closure delay larger than 1 ns.

Baseline	Number	Length (km)
FORTLEZA–KOKEE	1	11063
HART15M–YARRA12M	1	7848
KATH12M–NYALES20	1	10410
KOKEE–WESTFORD	1	7676
WESTFORD–WARK12M	1	11534
WESTFORD–YARRA12M	1	12638
FORTLEZA–ZELENCHK	3	8649
BADARY–FORTLEZA	4	11154
FORTLEZA–TSUKUB32	4	12252
KATH12M–ONSALA60	4	10928
KATH12M–WETTZELL	4	11026
TSUKUB32–WESTFORD	4	9505
BADARY–WESTFORD	5	8671
KATH12M–WESTFORD	5	12164
KATH12M–YEBES40M	5	11697
KOKEE–YEBES40M	5	10687
KATH12M–MATERA	6	10953
KOKEE–MATERA	6	10894
KOKEE–WETTZELL	9	10357
KOKEE–ONSALA60	15	9792
KOKEE–YARRA12M	32	9498

structure as well. It is worth noting that except for the baseline clock offset used to absorb constant biases between baselines, no other parameters in VLBI data analysis can absorb any part of the closure delay, which will finally impact the residuals. The observables with a large contribution to the closure delay are always identified as outliers during the data analysis. The study here shows that these observables are not outliers but are systematically affected by source structure.

The limitations of the application of equation (4) to the multiband group delay observable need to be discussed here. Finite bandwidth for multiband group delay contributes to errors in the modeled structure effects based on equation (4) because the structure changes with frequency and/or the change in resolution R as a function with frequency cause τ_s to change with frequency. The X band observations in CONT14 use 8 channels spread over 720 MHz, for a fractional bandwidth of 0.085. We have performed numerical simulations covering a large range of component separations, baseline lengths and orientations, and K values to study this effect. For the case of 0642+449, with $K \sim 0.9$ and the separation about 0.5 mas, we find a median absolute deviation between τ_s computed at the top and bottom of the observed X band frequencies, over the observed base-

line lengths and orientations, to be 2.6 fs, and the RMS deviation to be 11 ps, for two components with the same spectral index. With one component having a spectral index of 0 (typical for an AGN core) and the other component having a spectral index of -0.7 (typical for an optically thin jet component), the median absolute deviation and RMS are 40 fs and 14 ps, respectively. Hence, the finite bandwidth of the CONT14 observations analyzed here does not present a significant violation of the infinitesimal bandwidth assumption of equation (4) for this source. Furthermore, our simulations show that having reasonable different spectral indices for the two components contributes significantly less to differences in the structure delay with frequency than the changes in interferometer resolution (R) as a function of frequency (14 ps for spectral index and R changes together, compared to 11 ps for R changes alone).

7. CONCLUSION AND DISCUSSION

Closure delay analysis has several advantages for geodetic VLBI. First, it directly studies structure effects from the geodetic observables—the multiband group delays—themselves, the quantities actually used to determine station position and motions, Earth orientation parameters, and other astrometric/geometric parameters. Second, closure delay analysis can serve as an indicator to evaluate the performance of any structure model, whether that model is determined by fitting closure delays or through an imaging analysis. Third, model fitting of closure delays can identify the strongest components of a source while ignoring weak components that do not significantly alter the group delay, simplifying the analysis procedure. In contrast to many astrophysical studies where the weak components are of interest, geodetic VLBI analysis can often ignore such components. Fourth, a closure delay analysis can save time and effort in both processing and software development for geodetic purposes compared to standard VLBI imaging.

We showed that closure delays can determine the magnitude of the measurement noise in the geodetic VLBI observables, and thereby also determine the magnitude of structure effects in the geodetic VLBI observables. We also showed that large closure delays, even closure delays in excess of 10 ns, are related to source structure effects, and that the underlying delay measurements are not caused by simple measurement errors. We demonstrated for the first time that source structure can be obtained from the closure *delays* as opposed to closure phases or closure amplitudes from visibility data. For sources that are reasonably compact on short VLBI baselines, we can simply and directly solve for (not fit) structure effects for the entire VLBI network of baselines without any additional a priori information. We also ap-

ply model fitting to determine source structure, showing how closure delays can yield structure information without the need for sources to be unresolved on short baselines. This method is relatively simple to implement within existing geodetic analysis tools, uses input data from the standard geodetic database files, and does not require significant computational resources. For example, we can compute structure models for all sources in the 15-day CONT14 campaign in a fraction of an hour, whereas our current imaging analysis from the raw visibility data requires about 16 hours to process one 24-hour segment of the CONT14 campaign on a similar computer.

In an array of N antennas, with $N(N-1)/2$ interferometer baselines, there are $N(N-1)/2$ unknown structure effects to be determined and $(N-1)(N-2)/2$ independent closure delays as observables. Therefore, the fraction of the total structure delay information available in the closure delays is $(N-2)/N$. The ratio shows the benefits to be gained by increasing the number of antennas in the array; with only 4 antennas, 50% of the structure delay information is available, while for 15 antennas, as the case of CONT14 observations of source 0642+449, the ratio increases to 87%. From these observations, the source structure effect is demonstrated at the level of each individual VLBI group delay for the first time. The study reveals that at X band (8.4 GHz) during the CONT14 sessions the source had two point-like components with a flux-density ratio of 0.92, that is, almost equally bright. The position of the weaker component with respect to the stronger one is estimated to be $-426 \pm 12 \mu\text{as}$ in right ascension and $-66 \pm 19 \mu\text{as}$ in declination. Finally, the standard deviation of the corrected closure delay was reduced by 36%. This structure model agrees with the estimated source structure effect on baselines with lengths less than 10 000 km very well, but does not fit some of the longest baselines. There are mainly four reasons for that: (1) source structure effects on these longest baselines with $R \gtrsim 0.7$ are much more sensitive to the relative position of the two components; (2) such long baselines only have a few observations over one circle of uv position angle, making it statistically difficult to identify the variation caused by the source structure; (3) there can be structure at smaller scale that shows structure effect on longest baselines but none on baselines shorter than 10 000 km; and (4) the model of Equation (4) is the derivative of the structure phase with respect to the observing frequency, while the multiband group delay is derived from the linear estimation of the observed phase over 8 channels spanning about 0.7 GHz—application of this model for multiband group delays introduces errors in the structure effect, which may have larger impacts when the baseline length is longer than 11 000 km with $R \gtrsim 0.7$. Due to this in-

adequateness of the model for multiband group delays, the flux-density ratio K may have been underestimated.

In 1992 and 1995, this source was observed to have a compact “core-jet” morphology with the resolution of several milliarcseconds by [Gurvits et al. \(1992\)](#) and [Xu et al. \(1995\)](#), respectively. Recently, space VLBI (RadioAstron) observations of this source at 1.6 GHz in 2013 with a resolution of 0.8 mas, ~ 4 times better than that of ground VLBI images at this wavelength, found that this source has two compact cores separated by 0.76 mas with a position angle of 81° in the sky plane ([Lobanov et al. 2015](#)). Since space VLBI observations were made fourteen months earlier than CONT14 observations, one may not expect they were observing the same blob, but the position angle of two components should be approximately in the same direction. Our result demonstrates that the two components are in the direction of position angle about 261.2° , which is the same direction detected by space VLBI. The source 0642+449 did not exhibit a significant structure effect due to a frequency dependence of the flux densities of the two components, which has a completely different pattern, such as more peaks over 24 hours for baselines with $R \approx 0.5$. Our study shows a similar structure of this source with a resolution comparable to that of the space VLBI, demonstrating the feasibility of the application of astrometric observables for the study of the source structure with this method.

From the study by [Bertarini et al. \(2011\)](#), we expect polarization leakage to affect the multiband group delay by less than 1.6 ps for 90 % of the observations. General leakage of LCP into RCP for the geodetic observations will result in a baseline-dependent bias. For the LCP part of the Stokes I emission that leaks into RCP, these biases are constant in time and baseline orientation for a given station pair, and do not explain the large, systematic, and source-dependent effects. [Homan & Lister \(2006\)](#) showed that at VLBI resolutions, the fractional circular polarization of AGN core and jet components is typically less than about 1 %. Supposing that different baseline orientations constructively add/subtract the phases from two components that are circularly polarized at the 1 % level, the change in delay caused by circularly polarized source structure would only be 2 % of the change in delay for the Stokes I emission. We therefore expect that polarization effects are negligible for this study, although they may be important to reach picosecond accuracies.

The large closure delays have also been effectively traced, which reveals that most observables erroneously identified as outliers in VLBI data analysis are in fact exposed to the source structure effect and this effect could be at the level of tens of ns in some occasions even for a radio source with a rather flat spectral in-

dex. This cannot be explained yet by the model. This needs to be studied in the future to find the explanation from astrophysics, while for astrometric VLBI we should schedule routine observations more effectively to exclude this kind of radio source, or to observe it without such long baselines only if the two components do not move with each other.

It is still challenging to implement the identified source structure to correct the effect in VLBI data analysis. First, an accurate model for multiband group delays to the level of at least 10 ps needs to be derived. This model should be able to reduce the magnitudes of the closure delays of triangles with the longest baselines to the level of that of small triangles, a few tens of ps. Second, a careful re-study of the linear combination of S and X band data with the presence of source structure would be essential to have an accurate correction for the source structure effect on the combined S-X observable. Moreover, astrometric/geodetic VLBI observables at S band are one order of magnitude noisier than that at X band, which makes the source structure at S band almost unrecoverable, and the structures at S and X bands are different. In general, structures at S band are much more resolved than that at X band.

How could our method be improved for the study of source structure? First, there should be more effective ways of deriving the structure effects on $(N - 1)$ baselines. Due to the limitation from the assumption used for the connection, our method would confine to a small fraction of radio sources. But if one can develop a new way to break this limitation, our method may allow us to directly correct the structure delay on each single delay observable for geodetic VLBI data analysis. Second, one might develop a new method of image reconstruction in an iterative way other than modeling the structure delay. Then a non-linear estimation of the structure parameters from the closure delay has to be developed. The method can thus be extended to be used for more general cases, complex or resolved sources. The rigorous method to correct the structure effect is to make images

based on the standard VLBI imaging from the same observations and to correct the raw visibility phases for source structure in the geodetic VLBI analysis software prior to the multiband group delay fitting. Even though this will need more work and resource compared to the current procedure of the routine VLBI data analysis, the geodetic VLBI should move onto it in the near future. We are working on making images of CONT14 observations and the results will be presented in another paper.

This method could be of great help to monitor the performance of radio sources for the historical VLBI observations and the VLBI Global Observing System (VGOS; Petrachenko et al. 2009). In VGOS, there is a global network of well-distributed stations and particularly several twin telescopes. A wider range of baseline lengths from hundreds of meters will be available, which then will allow the source structure with a wide separation of compact components to be detectable. Moreover, if the point-like sources that are more likely to be observed in astrometric VLBI begin to demonstrate structure, it is likely to roughly model their structures as consisting of compact components rather than a flat brightness distribution. The source structure effect, as one of the main and inevitable problems for the goals of the VGOS, can be expected to be handled by this method to some extent. Besides the astrometric VLBI, the method can provide benefits as imaging for the astrophysical study of the source structure from continuous observations within VGOS.

We thank the IVS for the CONT14 data used in this work, and David Gordon (Goddard Space Flight Center, USA) and Brian Corey (MIT Haystack Observatory, USA) for the helpful discussions of calculating closure delay from geodetic VLBI observations. This work was done while M.H.X. worked as a guest scientist at GFZ, Germany, and supported by the National Natural Science Foundation of China (Grant No. 11473057 and 11303077).

REFERENCES

- Bertarini, A., Roy, A. L., Corey, B., et al. 2011, *Journal of Geodesy*, 85, 715
- Campbell, J., Schuh, H., & Zeppenfeld, G., 1988, in *The Impact of VLBI on Astrophysics and Geophysics*, IAU Symposium No. 129, ed. J.M. Moran, M.J. Reid (Reidel: Dordrecht), 427
- Charlot, P., Lestrade, J. F. & Boucher, C., 1988, in *The Impact of VLBI on Astrophysics and Geophysics*, IAU Symposium No. 129, ed. J.M. Moran, M.J. Reid (Reidel: Dordrecht), 33
- Charlot, P., 1990a, *A&A*, 229, 51
- Charlot, P., 1990b, *AJ*, 99, 1309
- Charlot P., 1993, in *EVGA 1993 General Meeting Proceedings*, 171, ed. J. Campbell & A. Nothnagel (Germany: Bad Neuenahr.)
- Charlot, P., 2010, *AJ*, 139, 1713
- Feissel-Vernier, M., 2003, *A&A*, 403, 105
- Fey, A. L., Clegg, A. W. & Fomalont E. B., 1996, *Astrophys. J., Suppl. Ser.*, 105, 299
- Fey, A. L., & Charlot, P. 1997, *ApJ*, 111, 95
- Fey, A. L., & Charlot, P. 2000, *ApJ*, 128, 17
- Fey, A., Gordon, D., Jacobs C. S., et al., 2015, *AJ*, 150, 58
- Fomalont, E., Johnston, K., Fey, A., et al., 2011, *AJ*, 141, 91
- Gontier A. M., Britzen S., Witzel A., et al. 1993, in *EVGA 1993 General Meeting Proceedings*, 167, ed. J. Campbell & A. Nothnagel (Germany: Bad Neuenahr.)
- Gurvits, L. I., Kardashev, N. S., Popov, M. V., et al. 1992, *A&A*, 260, 82

- Homan, D. C., & Lister, M. L. 2006, *AJ*, 131, 1262
- Jennison, R. C. 1958, *MNRAS*, 118, 276
- Kellermann K. I. & Owen F. N., 1988, *Galactic and Extragalactic Radio Astronomy*, (2nd ed.; The Observatory), Chapter 13
- Lister, M. L., Cohen, M. H., Homan, D. C., et al. 2009, *AJ*, 138, 1874
- Lister, M. L., Aller, M. F., Aller, H. D., et al. 2013, *AJ*, 146, 120
- Lobanov, A. P., Gómez, J. L., Bruni, G., et al., 2015, *A&A*, 583, A100
- Ma, C., Arias, E. F., Eubanks, T. M., et al., 1998, *AJ*, 116, 516
- MacMillan, D. S. & Ma, C., 2007, *J. Geod.*, 81, 443
- Malkin, Z., 2008, *J. Geod.*, 82, 325
- Moór A., Frey S., Lambert S., et al., 2011, *AJ*, 141, 178
- Nothnagel, A., 2015, *The IVS data input to ITRF2014*, International VLBI Service for Geodesy and Astrometry, DOI: <http://doi.org/10.5880/GFZ.1.1.2015.002>
- Ojha, R., Fey, A. L., Johnston K. J., et al., 2004, *AJ*, 127, 3609
- Ojha, R., Fey, A. L., Charlot, P., et al., 2005, *AJ*, 130, 2529
- Pearson, T. J., & Readhead, A. C. S. 1981, *ApJ*, 248, 61
- Pearson, T. J., & Readhead, A. C. S. 1984, *ARA&A*, 22, 97
- Pearson, T. J., & Readhead, A. C. S. 1988, *ApJ*, 328, 114
- Petrachenko, B., Niell, A., Behrend, D., et al. 2009, NASA/TM-2009-214180, <ftp://ivsc.gsfc.nasa.gov/pub/misc/V2C/TM-2009-214180.pdf>
- Petrov L., 2007, in 18th EVGA General Meeting Proceedings, 141, ed. J. Böhm, A. Pany, H. Schuh (Germany: Geowissenschaftliche Mitteilungen.)
- Piner, B. G., Mahmud, M., Fey, A. L., et al., 2007, *AJ*, 133, 235
- Plank, L., Shabala, S. S., McCallum, J. N., et al., 2016, *MNRAS*, 455, 343
- Readhead, A. C. S., & Wilkinson, P. N. 1978, *ApJ*, 223, 25
- Rogers, A. E. E., Hinteregger, H. F., Whitney, A. R., et al. 1974, *ApJ*, 193, 293
- Schuh, H. & Behrend D., 2012, *J. Geodyn.*, 61, 68
- Shabala, S. S., McCallum, J. N., Plank, L., et al., 2015, *J. Geod.*, 89, 873
- Sovers, O. J., Charlot, P., Fey, A. L., et al. 2002, in IVS 2002 General Meeting Proceedings, ed. N. R. Vandenberg & K. D. Baver (Japan)
- Tang & Rönnäng, 1988, in *The Impact of VLBI on Astrophysics and Geophysics*, IAU Symposium No. 129, ed. J.M. Moran, M.J. Reid (Reidel: Dordrecht), 431
- Taylor, G. B., Vermeulen, R. C., Pearson, T. J., et al., 1994, *ApJS*, 95, 345
- Thomas, J. B., 1980, "An analysis of source structure effects in radio interferometry measurements", JPL publication 80-84, JPL, Pasadena, California Dec 15
- Tornatore, V. & Charlot P., 2007, *J. Geod.*, 81, 469
- Ulvestad, J. L., 1988, in *The Impact of VLBI on Astrophysics and Geophysics*, IAU Symposium No. 129, ed. J.M. Moran, M.J. Reid (Reidel: Dordrecht), 429
- Whitney, A. R., Shapiro, I. I., Rogers, A. E. E., et al., 1971, *Sci*, 173, 225
- Xu, W., Readhead, A. C. S., Pearson, T. J., et al., 1995, *Astrophys. J., Suppl. Ser.*, 99, 297
- Zeppenfeld G., 1991, in EVGA 1991 General Meeting Proceedings, IV-16, (Netherland: Survey Department of Rijksw.)